Electrochimica Acta 162 (2015) 11–16

Contents lists available at ScienceDirect

Electrochimica Acta

journal homepage: www.elsevier.com/locate/electacta

Nanotubes for charge storage – towards an atomistic model

Leila Mohammadzadeh[a], Aleksej Goduljan[a], Fernanda Juarez[a], Paola Quaino[b], Elizabeth Santos[a,c], Wolfgang Schmickler[a,*]

[a] Institute of Theoretical Chemistry, Ulm University D-89069 Ulm, Germany
[b] PRELINE, Universidad Nacional del Litoral Santa Fe, Argentina
[c] Facultad de Matemática, Astronomía y Física, IFEG-CONICET Universidad Nacional de Córdoba, Córdoba, Argentina

ARTICLE INFO

Article history:
Received 13 August 2014
Received in revised form 3 December 2014
Accepted 6 December 2014
Available online 12 December 2014

Keywords:
Nanotubes
Charge storage
DFT
Image charge
Screening

ABSTRACT

We examine the insertion of alkali and halide ions into narrow nanotubes of graphite and gold by density functional theory (DFT). For tubes with diameters less than about 10 Åthe optimum position of the ion is in the center of the tube. Bader analysis and an analysis of the densities of states gave contradictory results for the charge on the halide ions, but we argue on physical grounds that they carry unit negative charge. We have calculated the energies of inserting the atoms into the tubes, where they are ionized. Because of the small system size the work function of the tubes changes during this process, which makes it difficult to interpret these energies. The surrounding tubes screen the ionic charge very effectively; thereby the ion-ion interactions are strongly reduced, which explains, why narrow tubes store charge more effectively than wider one. These effects are stronger for gold than for graphite tubes. We define an effective image radius of a cylindrical tube, and calculate the image energy experienced by the ions.

1. Introduction

The advent of nanotechnology has opened a new domain for electrochemistry, and electrode structures of nanometer size, such as pores and clusters, have become the subject of intensive investigations. They not only promise applications in catalysis, energy storage and conversion, but they also present challenges for fundamental science. A case in point is the double-layer structure in confined geometries such as nanopores. Conventional double-layer theory considers only semi-infinite electrolyte solutions, and even at high ionic concentrations the thickness of the double layer is of the order of 10 - 20 Å. This is larger than the dimensions of nanopores, which are often only a little wider than the diameters of ions or of water molecules. Obviously, simple continuum models like the Gouy-Chapman theory are useless in this case, and new models at the atomic level are called for.

In this work, we want to take a first step in this direction and consider a fundamental case, a single ion in a metal or carbon nanotube. Our work is partially motivated by recent experimental findings which indicate, that pores with radii that are so small, that solvated ions cannot enter, store charge more efficiently than wider pores – in other words, their double-layer capacity per unit area is larger [1,2]. Kondrat and Kornyshev [3] explained these unexpected findings by the image interaction between the ions and the walls of the pores. Based on these ideas, Rochester et al. [4] constructed a simple model, in which the walls of the pore were either taken to be a perfect classical metal or a Thomas-Fermi metal, and explained how the image interaction screens the Coulomb potential of a point charge and thus enables a denser packing of ions. While these explanations are certainly qualitatively correct, a description at the atomic level is missing. An important step in this direction has been taken by Merlet et al. [5] who studied the capacitance of nanoporous carbon by molecular dynamics using a corse-grained model of an ionic liquid, following earlier work by Shim and Kim [6] along the same line. We start at a more fundamental level and consider a single ion in a nanotube in order to understand its interaction with the tube and the screening of the charge. Therefore, we have performed DFT (density functional theory) calculations for a series of alkali and halide ions in nanotubes and investigated the image interaction and the concomitant screening of the Coulomb interaction quantitatively. First results for Na^+ and Cs^+ have been published in [7]; here we focus on Li^+, because of its importance in battery technology [8,9], present first results for anions, and provide details that were missing in the first paper. Again we shall contrast the behaviour of carbon tubes with that of gold tubes, since metals are known to screen charges much better than carbon [10,11]. For a related approach to lithium stored in graphite, see the very recent article of Robledo et al. [12].

* Corresponding author.
E-mail address: wolfgang.schmickler@uni-ulm.de (W. Schmickler).

http://dx.doi.org/10.1016/j.electacta.2014.12.031
0013-4686/

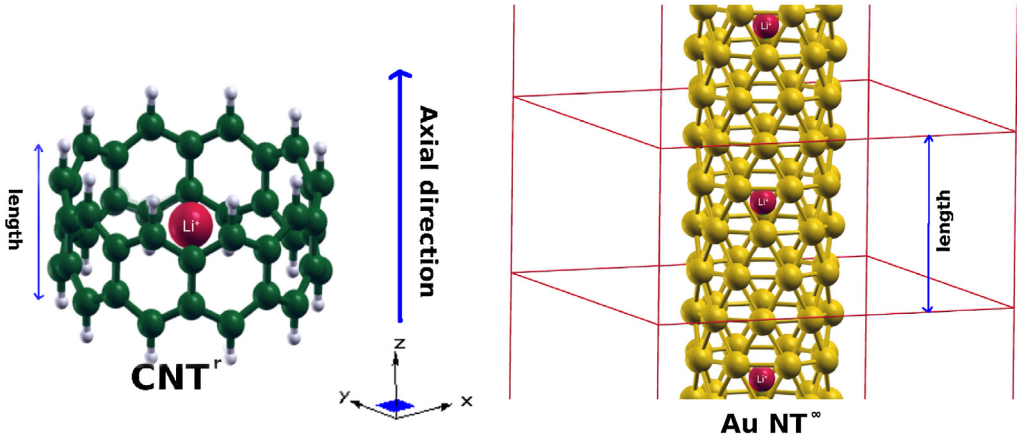

Fig. 1. Examples of lithium ions inside of gold nanotubes (right) and carbon rings (left) investigated. The red lines on the right represent the unit cell.

2. Details of the investigated systems

As in our previous publication [7] we have investigated atoms placed inside single-walled narrow carbon or gold nanotubes. In particular, we have studied alkali and halogen atoms placed into (6,6) and (8,8) gold nanotubes $(AuNT)^{\infty}$ – see [13,14], and (6,0), (8,0) and (10,0) carbon nanotubes $(CNT)^{r}$ [15]. For the $AuNT^{\infty}$ we have used cyclic boundary conditions to represent infinite tubes, indicated by the superscript ∞, while the CNT are of finite size in the axial direction (see Fig. 1), which we indicate by the superscript r for ring. The CNT^{r}s by themselves are not stable, therefore we saturated the dangling bonds with hydrogen atoms. For comparison we shall also present a few results for infinite (6,3)CNT^{∞}, but a thorough discussion of these tubes, which have metallic properties, will be left to a future publication. The dimensions of the investigated systems are given in Table 1; the technical details of the calculations will be presented in the appendix.

2.1. Technical Details

Periodic density functional theory (DFT) calculations based on plane waves have been performed as implemented in the DACAPO code [25]. The electron-ion interactions were accounted through ultrasoft pseudopotentials [26], while the valence electrons were treated within the generalized gradient approximation (GGA) in the version of Perdew, Burke and Ernzerhof (PBE) [27]. The electron wave functions were expanded in a plane-wave basis setup to a kinetic energy cutoff of 400 eV (450 eV for the density). Brillouin zone integration was performed using the Gamma point. Spin polarization was considered in all the systems, but the results showed no net spin. Infinite CNTs were also calculated using the same computational parameters in the VASP code [28]. The obtained results were similar. For the relaxations the convergence criterion was achieved when the total forces were less than 40 meV/Å. Infinite gold nanotubes with and without ions were fully relaxed, as well as the hydrogenated and infinite carbon nanotubes.

All the systems used were neutral, but we confirmed the loss or gain of charge in the central atom by using Bader analysis method [17]. We used a dipole-correction scheme [29] in the systems that are not completely symmetric, in order to have a well-defined vacuum potential. The electrostatic part (ionic and Hartree potentials) of the local potential was calculated, but the exchange-correlation was not added. For the examination of the properties of a system this is more desirable due to the fact that the electrostatic potential converges more rapidly to the vacuum level than the total potential.

Table 1
Dimension of the empty tubes. In the carbon tubes the number of hydrogen atoms that saturate the dangling bonds equals half the number of carbon atoms. For the gold tubes the length corresponds to the length of the unit cell.

system	C atoms	diameter/nm	length/nm
(6,0)CNT^{r}	24	0.484	0.500
(8,0)CNT^{r}	32	0.637	0.500
(10,0)CNT^{r}	40	0.789	0.500
	Au atoms	diameter/nm	length/nm
(6,6)$AuNT^{\infty}$	24	0.545	0.960
(8,8) $AuNT^{\infty}$	32	0.732	0.969

3. Results and discussion

3.1. Cation insertion

We have studied lithium, sodium, and cesium atoms, but we focus on lithium, which had not been included in our first report [7]. Initially we placed a neutral atom in the center. At the end of the calculations, in all cases we discuss here, the Bader charge on the ion was +1 within DFT error, and the stable position was at the center of the ring. Table 2 gives the insertion energies defined as:

$$E_{\mathrm{ins}} = E(\mathrm{tube} + \mathrm{ion}) - E(\mathrm{tube}) - E(\mathrm{atom}) \quad (1)$$

In our previous article we have argued that, in the absence of chemical interactions, the insertion energies should obey the equation:

$$E_{\mathrm{ins}} = I_1 - \Phi + E_{\mathrm{im}} \quad (2)$$

where I_1 is the first ionization energy (5.41 eV for Li), Φ is the work function of the tube, and E_{im} is the image energy. This equation immediately explains, why the insertion energies in the gold tubes are more favorable than in the CNT, since metals screen an external charge much better than carbon and hence provide larger image energies. However, it does not explain the small values for the CNT, nor the rather unsystematic variation with size. The application of this equation is straightforward only for real infinite tubes, where the work function does not change when an electron is transferred. In the finite systems considered here the work function becomes lower, as the electron is transferred from the alkali atom to the tube. The same argument applies to the infinite $AuNT^{\infty}$, since in this case

Table 2
Insertion energies for Li^{+} in various nanotubes.

system	(6,0)CNT^{r}	(8,0)CNT^{r}	(10,0)CNT^{r}	(6,6)$AuNT^{\infty}$	(8,8)$AuNT^{\infty}$
E_{ins}/eV	−0.1	−0.29	−0.20	−2.39	−2.51

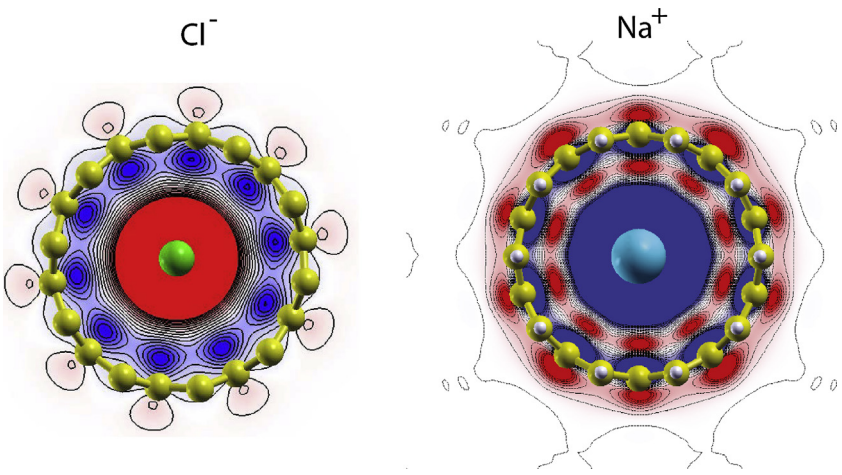

Fig. 2. Charge difference plots for a chlorine and a sodium atom in a (10,0) CNT^r. Red (blue) indicates an excess of negative (positive) charge.

Table 3
Insertion energies E_{ins} and the difference $(E_{ins} - I_1)$ for alkali ions in (10,0) CNT^r.

	Li^+	Na^+	Cs^+
E_{ins}/eV	−0.2	−0.64	−2.0
$(E_{ins} - I_1)$/eV	−5.60	−5.78	−5.89

Table 4
Insertion energies E_{ins} and the difference $(E_{ins} - I_1)$ for alkali ions in (6,3)CNT$^\infty$.

	Li^+/(6,3)CNT$^\infty$	Na^+/(6,3)CNT$^\infty$
E_{ins}/eV	−1.07	−1.17
$(E_{ins} - I_1)$/eV	−6.47	−6.31

one electron is transferred per unit cell. This effect is the greater, the smaller the tube, and is also greater for the CNTs considered here: the (8,0) and the (10,0) CNT^{r}s are semiconductors even when they are infinite, and the (6,0)CNT^r, which would be metallic if it were infinite, is greatly affected by charging because of its small size [20,21]. Since it is impossible to follow the charging with DFT, we cannot deduce the image energies. Below we shall show how they can be obtained by a different route.

This change of the work function upon charging should depend only on the size of the ring, not on the nature of the ion. We can therefore compare the insertion energies of various cations in a ring of given size. According to eq. (2) the difference $(E_{ins} - I_1)$ should be constant, since the image energy should depend on the size of the ring only. Table 3 shows the results for the (10,0)CNT^r, the largest tube we investigated; for this tube there are no deformation effects for Cs. Within the usual DFT accuracy, the difference $(E_{ins} - I_1)$ is indeed almost constant.

As discussed above, the nanotubes discussed so far are semiconducting, so that the electron is transferred from the alkali atom to the conduction band of the ring. In contrast the chiral (6,3)CNT$^\infty$ show a metallic conductivity; therefore we expect the insertion energies into these tubes to be substantially larger. This is indeed so (see Table 4); the two alkali ions investigated in this system also obey the relation $(E_{ins} - I_1) \approx \text{const}$.

3.2. Results for anions

It is of great interest to contrast the insertion of cations with those of anions. We have therefore performed calculations for Cl, Br, and I in order to see, if their behavior differs essentially from that of the alkali ions. Explicit calculations were performed for (10,0)CNT^r.

All anions are stable at the center of the tube. The charge difference plots, shown in Fig. 2, look similar to those for the alkalis, but with the sign of the charges interchanged. In both cases one sees the ion in the center surrounded by its image charge, which is localized near the carbon atoms, but somewhat closer to the ion in the center.

Table 5
Bader charges, energies of insertion E_{ins}, electron affinities E_A, and the sum $E_{ins} + E_A$ for several halide atoms in (10,0)CNT^r. All energies are in eV. As explained in the text, we think that the Bader charges are misleading.

atom	Cl	Br	I
Bader charge	−0.70	−0.66	−0.58
E_{ins}	−1.49	−1.22	−0.85
E_A	4.63	3.37	3.07
$E_{ins} + E_A$	2.14	2.15	2.22

For an interpretation of the results it is of great importance to know the charge on the anions. The position at the center of the tubes indicates that the ions are not chemically bonded to the tubes; so there is little electronic overlap, and the charge should be well defined. However, as recently discussed by our group [16], charge analysis based on DFT calculations can result in artificial partial charges distributed on atoms that are not chemically bonded. There are various ways to obtain charges from DFT; we have performed a Bader analysis [17] and obtained partial charges for all anions (see Table 5), whose absolute value decreases slightly down the periodic table. However, the electronic densities of states (DOS) show a different result. In all cases investigated, the DOS of the p electrons of the halides are almost completely filled, indicating that the charge on the ion is close to -1. Fig. 3 shows this for the case of Br^-; conversely, the DOS of the Na^+ 3s orbital lies above the Fermi level and is empty.

The charge analysis based on DFT results being contradictory, we shall try to determine the charge through a physical argument based on energies – after all, DFT has been optimized to give the correct energies. If charge transfer were complete, and the energetics governed by electrostatics, they would be given by:

$$E_{ins} = \Phi - E_A + E_{im} \qquad \text{complete charge transfer} \qquad (3)$$

where E_A is the electron affinity. Since the image energy should depend on the size of the ring only, this would imply that the sum $E_{ins} + E_A$ is constant – and this is indeed the case (see Table 5). Given the different sizes and insertion energies, this is unlikely to be a coincidence. Also, as we shall see below, the Coulomb potential generated by the ions also indicates that they are fully ionized. Therefore we shall assume in the rest of this article that the halide ions carry unit negative charge.

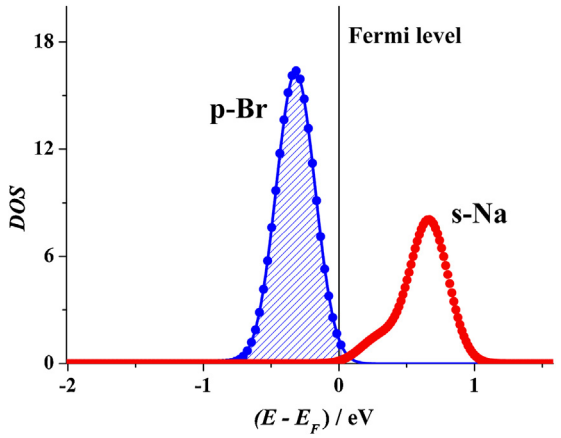

Fig. 3. Densities of states for a Na^+ and a Br^- ion placed inside a (10,0)CNT^r

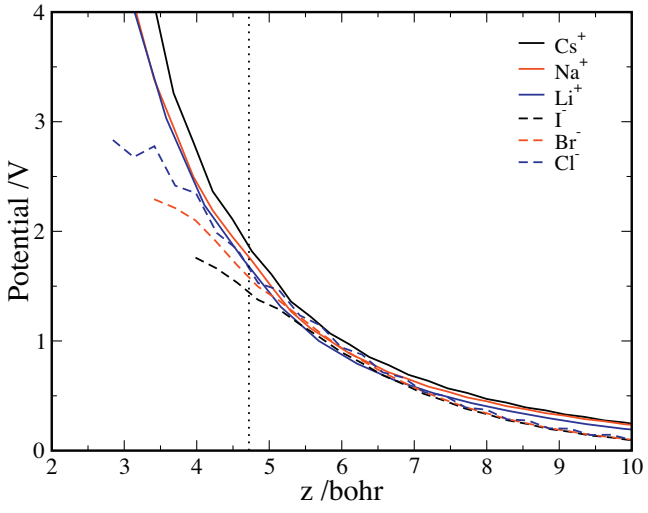

Fig. 4. Screened Coulomb potential along the axis of (10,0)CNT^r as a function of the distance from the ion. The vertical dotted line indicates the end of the ring.

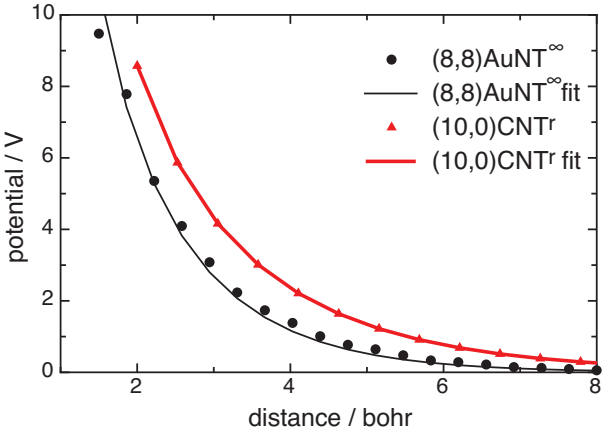

Fig. 5. Screened Coulomb potential along the axis of the tube as a function of the distance for a (8,8)$AuNT^\infty$ and a (10,0)CNT^r as obtained by DFT, and the corresponding curves obtained by fitting the data to eq. (4) in order to obtain the effective image radius.

So why is it so simple to obtain the charges for the cations, and so difficult for the anions? In Bader analysis the estimation of the charges is based on a division of the electronic density and its attribution to specific atoms, which always involves an element of arbitrariness. [18,19]. For the cations the situation is simpler since an electron is missing, and the electronic density in the center is lower. In the case of the anions the electronic density within the tube is high, and there is no strict criterion to attribute it to the halide atom or to the carbon ring. In essence: it is easier to observe that something is missing, than to divide something that is present into various parts.

In principle, we could calculate the image energies E_{im} from eq. (3). However, just like eq. (2) this equation holds exactly only for an infinite tube, whose workfunction does not change when it is charged. Our calculations are for a finite ring, and the value of the workfunction changes during charging; here it should increase as the anions are charged, since electrons are taken away from the tube; therefore we refrain from trying to calculate the image energy from eq. (3).

3.3. Screening of the Coulomb potential

The Coulomb potential generated by the ion along the axis of the tube determines the interaction with other ions. Kondrat and Kornyshev [3] pointed out that this potential is strongly screened by the image force, and we have confirmed this by DFT calculations in our previous publication [7]. We have repeated these calculations for the anions and for Li^+. Fig. 4 shows the screened Coulomb potential along the axis of a (10,0)CNT^r for all ions investigated. At short distances the potentials of the anions differ a little because of the extended radii of the p orbitals, which increase down the periodic table. Otherwise the potentials for all particles are the same within DFT accuracy. Only at large distances there may be a small difference between the cations and the anions, the potential of the former decaying somewhat more slowly. This could be caused by the polarizability of the large anions.

3.4. Effective position of the image charge

In double layer theory the *apparent position of the image plane* x_{im} plays an important role: it characterizes the effect of the electrode on the double layer capacity. In essence, the response of the electrode is like that of a classical metal whose surface is at the position x_{im} [22]. For a nanotube, the corresponding concept is the effective radius of the image cylinder surface R_{im}, which we define as the cylindrical classical metal surface, which would generate the same potential along the axis as the real tube. For a classical cylindrical metal tube of radius R the potential on the cylinder axis is given by [4,23]:

$$\Phi(z) = \frac{2}{R} \sum_{m=1}^{\infty} \frac{\exp(-k_m z/R)}{k_m |J_1(k_m)|^2} \qquad (4)$$

where z is the distance from the center of the ion, k_m denotes the roots of the Bessel function $J_0(k_m) = 0$, and J_1 is the Bessel function of first order. The effective image radius R_{im} can be obtained by fitting the radius R from eq.(4) to the potential curve obtained by DFT as shown in Fig. 4. As can be seen from Fig. 5, the fit is quite good, and enables us to characterize the screening properties of various nanotubes.

In Table 6 we have collected the screening properties of various nanotubes. The characteristic property is the difference between the radius R of the tube, defined by the position of the nuclei, and the image radius R_{im}. The larger this difference, the better is the screening; it decreases, as the rings become smaller since there are fewer electrons to screen the charge. As we observed before [7], gold as a metal screens the charge much better than carbon. Note that the (8,8)$AuNT^\infty$ screens the charge better than the thinner (6,6)$AuNT^\infty$, because it has more electrons. For comparison we also give the distance between the effective image plane of Au(111) and

Table 6
Dimensions, effective image radii, and classical image energies for univalent ions in various nanotubes.

system	R_{im}/nm	R/nm	$(R-R_{im})$/nm	E_{im}/eV
(10,0)CNT^r	0.238	0.395	0.157	−2.64
(8,0)CNT^r	0.190	0.316	0.126	−3.33
(6,0)CNT^r	0.138	0.240	0.102	−4.63
(8,8)Au$^\infty$	0.178	0.366	0.188	−3.53
(6,6)Au$^\infty$	0.144	0.272	0.128	−4.36

the first layer of Au atoms: it is 2.06 Å, and thus still a little larger than the corresponding distance $R-R_{im}$ in the thickest gold tube investigated. We note in passing, that for planar metal surfaces the image plane is usually not referred to the first layer of atoms, as we did here, but to the conventional surface, which lies half a lattice spacing in front of the first layer of ions.

3.5. Image energies

The calculation of the effective image radii makes it possible to estimate the image energy experienced by the ions. For a unit point charge at the center of a tube with radius a the image energy can be obtained from elementary electrostatics. Using atomic units it is given by:

$$E_{im} = -\frac{1}{\pi a}\int_0^\infty \frac{K_0(x)}{I_0(x)}dx \approx \frac{-0.436}{a} \quad (5)$$

where K_0 and I_0 denote the corresponding Bessel functions. The resulting energies are given in the last column of Table 6; they are of the order of a few eV, and become more negative as the radius of the tube becomes smaller – with the exception of (6,6)AuNT$^\infty$ for reasons mentioned above. These energies should be compared with the free energies of solvation, which for a Li^+ ion in aqueous solution is of the order of -5.4 eV. When an ion enters from the bulk of the solution into these narrow tubes, it loses a sizable part of its solvation sheath, but gains the image energy; in addition, the ion in the tube interacts with the electrode potential, which can change the energy by an amount of the order of electron volts. Obviously, in order to obtain a more exact estimate of the energy of transfer from the bulk of the solution into a nanotube, on has to perform calculations for ions and solvent within the tubes.

3.6. Relation to Thomas-Fermi model

In a perfect metal the image plane is identical with the metal surface. The Thomas-Fermi model is a simple model for a non-perfect metal, in which an electric field can penetrate the electrode surface, and decays exponentially with the Thomas-Fermi length L; in this case the effective image plane lies a distance L behind the metal surface [24]. As mentioned above, on planar surfaces of a bulk metal the conventional surface lies half a lattice spacing in front of the first layer of atoms. In real metals, the effective position of the image plane lies in front of the metal surface, so that the Thomas-Fermi model cannot be applied – it would correspond to a negative Thomas-Fermi length, which is unphysical. However, on graphite the image plane lies behind the metal surface, so that the Thomas-Fermi model can be applied in a qualitative way. However, because of the strong nonlinear response of graphite, the application requires a length L which depends on the strength of the external field or, equivalently, the surface charge density.

On single wall carbon nanotubes the conventional definition of the surface cannot be applied, since there is no lattice. Therefore, it is customary to take the cylinder, on which the atoms lie, as the surface. As we have shown above, the effective image cylinder lies inside this surface, so the Thomas-Fermi model cannot be applied. However, this may be different for multiwalled nanotubes, where the conventional definition of the surface may be used. We think, that for mesoscopic models it is best to use the effective image radius calculated by our procedure, and use classical electrostatics.

4. Conclusions

In this work we have continued our investigation of ion insertion into narrow nanotubes by DFT with the aim to understand the double layer in confined electrochemical systems. In particular we considered alkali and halide ions, and contrasted the screening properties of carbon and gold nanotubes. As expected, the gold tubes screen external charges much better than the carbon tubes. In all cases considered, the position of the ions was stable at the center of the tube. For the cations it was easy to determine that they carry unit positive charge. In contrast, Bader analysis indicated partial negative charges on the halogens. However, physical reasoning based on the energetics and the screening properties, indicate a negative unit charge on the anions. An interpretation of the energies of insertion is rendered difficult by the fact that in the small systems considered the work function of the tubes changes as they are charged or discharged. In the electrochemical situation the ions already enter as ions into the tubes; therefore the most important energy is the image energy which the ions experience inside the tube. We managed to calculate these energies by an indirect route: First we obtained the effective image radius of the tube, which characterizes their screening properties, and from these we obtained the image energies. They are of the order of several electron volts, and thus of the same order of magnitude as the hydration energies of simple ions.

Our results explain, why narrow tubes store ions more effectively than wider tubes: The image energy lowers the energy of the ions inside the tube, and the screening of the charge lowers ion-ion interactions substantially. Our work should be considered as a first, successful step towards a model for the double layer in narrow tubes and pores.

Acknowledgments

We thank Prof. Dr. A. Kornyshev from Imperial College, London, for very useful discussions. Financial supports by the Deutsche Forschungsgemeinschaft (FOR 1376), and by an exchange agreement between the DAAD-Mincyt are gratefully acknowledged. P.Q., E.S. and W.S. thank CONICET for continued support. E. S. acknowledges PIP-CONICET 112-2010001-00411, and PICT- 2012-2324 (Agencia Nacional de Promoción Científica y Tecnológica, FONCYT, préstamo BID) for support, while P.Q. thanks CAID 501 201101 00276 LI UNL for support. A generous grant of computing time from the Baden-Württemberg grid is gratefully acknowledged.

References

[1] J. Chmiola, G. Yushin, Y. Gogotsi, C. Portet, P. Simon, P. Taberna, Science 313 (2006) 1760.
[2] C. Largeot, C. Portet, J. Chmiola, P-L. Taberna, Y. Gogotsi, P. Simon, J. Am. Chem. Soc. 130 (2008) 2730.
[3] S. Kondrat, A. Kornyshev, J. Phys.: Condens. Matter 23 (2011) 022201.
[4] C. Rochester, A. Lee, G. Pruessner, A. Kornyshev, ChemPhysChem 14 (2013) 4121.
[5] C. Merlet, B. Rotenberg, P.A. Madden, P.L. Taberna, P. Simon, Y. Gogotsi, M. Salanne, Nature Mat. 11 (2012) 306.
[6] Y. Shim, H.J. Kim, ACS Nano 4 (2010) 2345.
[7] A. Goduljan, F. Juarez, L. Mohammadzadeh, P. Quaino, E. Santos, W. Schmickler, Electrochem. Comm. 45 (2014) 48.
[8] V. Etacheri, R. Marom, R. Elazari, G. Salitra, D. Aurbach, Energy Environ. Sci. 4 (2011) 3243.
[9] K.E. Aifantis, S.A. Hackney, R.V. Kumar, High Energy Density Lithium Batteries, Wiley-VCH, Germany, 2010.
[10] N.B. Luque, W. Schmickler, Electrochim. Acta 71 (2012) 82.
[11] H. Gerischer, J. Phys. Chem. 89 (1985) 4249.

[12] C.B. Robledo, M. Otero, G. Luque, O. Cámara, D. Barraco, M.I. Rojas, E.P.M. Leiva, Electrochim. Acta (2014) http://dx.doi.org/10.1016/j.electacta.2014.07.013
[13] Y. Oshima, A. Onga, K. Takayanagi, Phys. Rev. Lett 91 (2003) 205503.
[14] F. Tielens, J. Andrés, J. Phys. Chem. C 111 (2007) 10342.
[15] R.T. Senger, S. Dag, S. Ciraci, Phys. Rev. Lett. 93 (2004) 196807.
[16] P. Quaino, N.B. Luque, G. Soldano, R. Nazmutdinov, E. Santos, T. Roman, A. Lundin, A. Groß, W. Schmickler, Electrochim. Acta 105 (2013) 248.
[17] (a) R.F.W. Bader, P.E. Cade, P.M. Beddall, J. Am. Chem. Soc., 93 (1971) 3095. (b) G. Henkelman, A. Arnaldsson, H. Jonsson, Comput. Mater. Sci. 36 (2006) 354.
[18] C. Fonseca Guerra, J.W. Handgraaf, E.J. Baerends, F.M. Bickelhaupt, J. of Comp. Chem. 25 (2003) 189.
[19] M.F. Juarez, E. Santos, J. of Phys. Chem. C 117 (2013) 4606.
[20] T.W. Ebbesen, H.J. Lezec, H. Hiura, J.W. Bennet, H.F. Ghaemi, T. Thio, Nature 382 (1996) 54.
[21] S. Fujita, A. Suzuki, Electrical Conduction in Graphene and Nanotubes, Wiley-VCH, Weinheim, 2013.
[22] W. Schmickler, D. Henderson, Progress in Surface Science 22 (4) (1986) 323–420.
[23] W.K.H. Panofsky, M. Phillips, Classical Electricity And Magnetism, Addison-Wesley Pub. Co., Reading, Massachusetts, 1962.
[24] A. Kornyshev, W. Schmickler, M. Vorotyntsev, Phys. Rev. B 25 (1982) 5244.
[25] B. Hammer, L.B. Hansen, J.K. Nørskov, Phys. Rev. B 59 (1999) 7413.
[26] D. Vanderbilt, Phys. Rev. B 41 (1990) 7892.
[27] J.P. Perdew, K. Burke, M. Ernzerhof, Phys. Rev. Lett. 77 (1996) 3865.
[28] G. Kresse, and J. Hafner, Phys. Rev. B 47 (1993) 558. (b) G. Kresse, and J. Hafner, Phys. Rev. B, 49 (1994) 14251.
[29] L. Bengtsson, Phys. Rev. B 59 (1999) 12301.